ISSN 1392-1207. MECHANIKA. Vol. 32, No. 5, 2026: 427–433

Numerical Simulation of Heat Conduction in Multi-Layer Plate Thermal Insulation Structures Based on Explicit Finite Difference Method

Jiabo WANG*, Jianghong MA*, Gaobin XUE*, Penggang YANG*, Peiyuan ZHAO*, Ruiying YU*, Ran YANG**

**Xihe Advanced Material Co., Ltd., Shanxi, Xi'an 710025, China*

***School of Intelligent Manufacturing, Qingdao Huanghai University, Shandong, Qingdao 266500, China, E-mail: yangran0206@163.com (Corresponding Author: Ran YANG).*

https://doi.org/10.5755/j02.mech.45845

1. Introduction

With the rapid development of modern military equipment toward hypersonic speeds, high maneuverability, and high power density, thermal protection has become a critical technical bottleneck limiting equipment performance, operational reliability, and service safety. For hypersonic aircraft, severe aerothermal heating induces extreme thermal loads on leading edges, inlets, and other key components during high-speed flight [1, 2]. Missile systems also require high-efficiency thermal insulation to guarantee in-service structural stability [3]. The cabin temperature of armored vehicles often exceeds the allowable thresholds for electronic components and crew thermal comfort, severely compromising the sustained combat capability of military equipment [4]. Furthermore, ammunition stored and transported in high-temperature environments experiences continuous thermal accumulation, which may trigger chemical instability and pose safety hazards [5]. Such extreme operating conditions impose stringent requirements on thermal insulation materials and structures for lightweight design, high-temperature resistance, efficient thermal insulation, and structural reliability.

Composite thermal insulation materials have emerged as the core research and engineering direction in military thermal protection due to their low density, low thermal conductivity, superior high-temperature resistance, and design flexibility [6, 7]. Multi-layer composite thermal insulation systems can effectively reduce the additional structural weight of thermal protection structures [8]. Specially designed porous structures suppress internal gas conduction and convection, yielding an equivalent thermal conductivity lower than that of static air under atmospheric conditions [9]. The layered structural configuration can flexibly adapt to the thermal insulation and mechanical performance demands of diverse engineering scenarios [10]. Heat transfer in practical service environments is inherently unsteady, and steady-state design indicators alone cannot guarantee the operational effectiveness of thermal insulation structures under full mission profiles [11]. Unsteady heat-transfer numerical simulation can reproduce the transient temperature response and heat evolution within thermal insulation layers under time-varying thermal loads. It enables the prediction of thermal insulation performance and potential thermal failure risks at the preliminary design stage, thereby significantly shortening the research and development cycle and reducing experimental costs [12, 13]. Therefore, the development of high-efficiency parametric simulation methods for unsteady heat conduction has become an urgent requirement for the optimal design of thermal insulation structures.

Domestic and international scholars have conducted extensive theoretical and experimental investigations into the heat-transfer characteristics of composite thermal insulation materials. Systematic heat transfer models have been established for multi-layer thermal insulation systems [14, 15]. Experimental testing methods have been developed to obtain accurate thermal conductivity and thermal diffusivity data across temperatures ranging from cryogenic to ultra-high [16]. Previous studies have revealed the mechanisms by which multiple factors influence thermal insulation performance and have proposed mixing rules, effective medium theory, and multi-scale homogenization methods to predict the thermophysical properties of composite materials [17, 18]. These research outcomes provide fundamental physical mechanisms and key material parameters for numerical thermal simulations. Using commercial numerical platforms such as ANSYS, COMSOL, and Abaqus, as well as self-compiled programs, researchers have performed numerous steady and unsteady thermal analyses that precisely characterize the evolution of the transient temperature field and the thermal stress distribution in thermal insulation structures [19, 20, 21]. Surrogate modeling has also been investigated for the multidisciplinary optimization of thermal protection systems [22, 23].

Existing general-purpose simulation platforms offer broad modeling capabilities, but repeated model setup can be inconvenient for screening one-dimensional multilayer configurations. This motivates a dedicated parametric tool that accepts layer thickness, thermophysical properties, and boundary conditions and returns transient temperature fields. The present study develops such a tool and compares its predictions with an Abaqus finite element model for a prescribed bilayer conduction problem. The scope is numerical implementation and inter-solver comparison; experimental validation and performance under realistic service conditions remain outside the present study.

2. Design and Implementation of Parametric Numerical Simulation Program

To address the one-dimensional unsteady heat conduction problem in multilayer flat structures in practical engineering, this study developed a dedicated numerical simulation program based on the explicit finite-difference method (FDM). Adopting an object-oriented programming framework, the program supports arbitrary combinations of multilayer materials, diverse boundary conditions, and time-

varying temperature boundary conditions. An intuitive graphical user interface (GUI) based on PySide6 was integrated to enable full-process parametric calculation and visualization of results.

2.1. Overall program architecture

The overall structural framework and operational logic of the developed program are illustrated in Fig. 1.

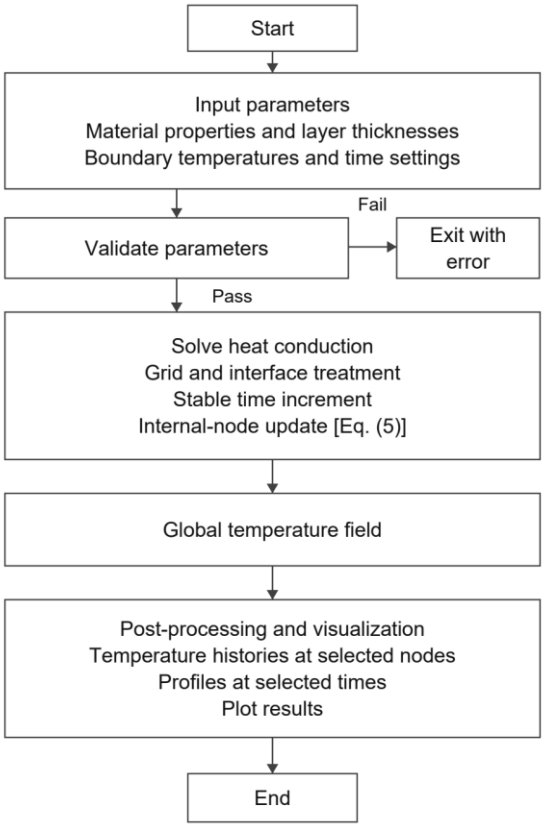

Fig. 1 Program framework

2.2. Governing equations and numerical methods

2.2.1. Governing equation of heat conduction

The governing equation for one-dimensional unsteady heat conduction without internal heat sources is given by Eq. (1).

$$\rho c \frac{\partial T}{\partial t} = \frac{\partial}{\partial t}\left(k \frac{\partial T}{\partial x} \right), \tag{1}$$

where ρ is the material density, kg/m³, c is the specific heat capacity, J/(kg·K), k is the thermal conductivity, W/(m·K), T is temperature, °C, t is time, s, and x is the spatial coordinate, m.

Within each homogeneous, isotropic layer with constant thermophysical properties, the thermal diffusivity is $\alpha = k/(\rho c)$, and Eq. (1) reduces to Eq. (2). This reduction does not apply across a discontinuity in thermal conductivity without a separate interface treatment.

$$\frac{\partial T}{\partial t} = \alpha \frac{\partial^2 T}{\partial x^2}. \tag{2}$$

2.2.2. Explicit finite difference scheme

The Forward-Time Central-Space (FTCS) explicit discretization scheme was adopted in this study. The first-order forward difference was employed for the discretization of the time derivative, as presented in Eq. (3).

$$\left.\frac{\partial T}{\partial t}\right|^n \approx \frac{Ti^{n+1} - T_i^n}{\Delta t}. \tag{3}$$

The second-order central difference scheme was applied to discretize the spatial second derivative, as shown in Eq. (4)

$$\left.\frac{\partial^2 T}{\partial x^2}\right|_i^n \approx \frac{T_{i+1}^n - 2T_i^n + T_{i-1}^n}{(\Delta x)^2}. \tag{4}$$

By substituting the above difference schemes into the heat conduction governing equation, the explicit iterative calculation formula was derived as follows:

$$T_i^{n+1} = T_i^n + Fo\left(T_{i+1}^n - 2T_i^n + T_{i-1}^n\right), \tag{5}$$

where the Fourier number is defined as $Fo = \alpha\Delta t / (\Delta x)^2$, a dimensionless parameter characterizing heat conduction intensity.

2.2.3. Stability criterion

For a uniform grid within a homogeneous layer, the explicit FTCS scheme is conditionally stable, with the standard interior-node criterion given by Eq. (6)

$$Fo \le \frac{1}{2}. \tag{6}$$

That is, the time step must satisfy:

$$\Delta t \le \frac{(\Delta x)^2}{2\alpha_{max}}. \tag{7}$$

For the uniform-grid case, the program calculates a nominal time-step limit from the grid spacing and maximum layer diffusivity and applies a factor of 0.8. This safety factor addresses the stated interior-node stability limit; it does not establish temporal convergence or independently verify the interface and boundary updates.

2.2.4. Boundary condition treatment

Asymmetric boundary conditions were applied on the two sides of the computational domain. The left boundary adopted the first-type Dirichlet boundary with time-varying wall temperature $T(0, t) = T_{left}(t)$, which supports constant temperature, linear temperature variation, periodic fluctuation, and arbitrary user-defined thermal loads. The right boundary was set with two optional boundary types:

the adiabatic Neumann boundary with zero heat flux $\delta T / \delta x| = 0$ which was numerically solved via the one-sided zero-gradient approximation with $T_N^{n+1} = T_{N-1}^{n+1}$; and the constant-temperature Dirichlet boundary $T(L, t) = T_{right}$.

2.2.5. Multi-layer interface treatment

Perfect thermal contact is assumed between adjacent layers, requiring continuity of temperature and normal heat flux at each interface. The program assigns material properties to grid nodes. Property assignment alone, however, does not establish heat-flux continuity when conductivity is discontinuous. The interface update must be consistent with the conservative form of Eq. (1), and its adequacy must be assessed independently of the homogeneous-layer FTCS formula.

3. Case Analysis of Heat Transfer Characteristics of Composite Thermal Insulation Structures

3.1. Performance parameters and setting of composite structures

A representative double-layer composite thermal insulation structure with a total thickness of 8 mm was selected as the research object. The structure consisted of a 2 mm-thick high-temperature-resistant ceramic matrix layer and a 6 mm-thick nano-aerogel composite layer with high-efficiency thermal insulation. The detailed thermophysical parameters of each structural layer are listed in Table 1.

Table 1

Material parameters of thermal insulation structure layers

No.	Thermal conductivity k, W/(m·K)	Density ρ, kg/m³	Specific heat capacity c, J/(kg·K)	Thickness s, mm
1	0.55	1700	900	2
2	0.06	400	1000	6

3.2. Boundary and initial condition settings

The initial temperature was 25°C throughout the domain before the boundary step. For $t > 0$, the left surface was prescribed at 100°C and the right surface was adiabatic. The simulation duration was 10 s. The stated uniform FDM grid spacing was 0.5 mm, giving 17 nodes over the 8 mm thickness. Using the maximum layer diffusivity and the 0.8 safety factor gives a nominal time step of approximately 0.278 s. The final integration step must be adjusted, or a smaller uniform step selected, to end exactly at 10 s.

The thermal diffusivities calculated from Table 1 are 3.595×10^{-7} m$^2/s$ for layer 1 and 1.500×10^{-7} m$^2/s$ for layer 2. The second value is approximately 42% of the first. The greater thickness and lower thermal conductivity of the insulation layer give it the larger thermal resistance, while its diffusivity characterizes the rate of transient temperature redistribution.

3.3. Temporal and spatial evolution laws of the temperature field

3.3.1. Spatial distribution characteristics of temperature

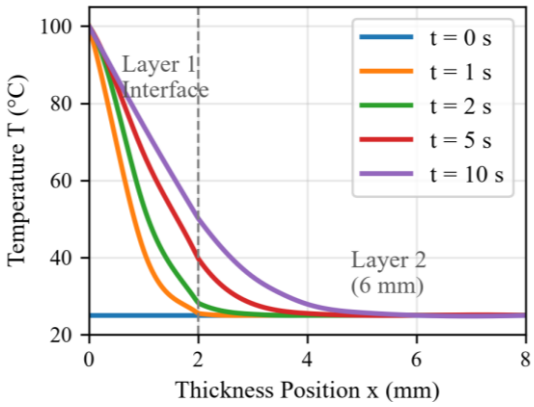

Fig. 2 Temperature distribution along the thickness at different moments

Fig. 2 presents the thickness-direction temperature distribution curves of the composite structure at five typical transient moments (t = 0 s, 1 s, 2 s, 5 s, 10 s).

Fig. 2 shows the gradual inward diffusion of heat after the hot-surface temperature step. The initial curve represents the temperature before application of that step. At later times, the calculated temperature rise is concentrated near the heated surface and decreases with depth. The reported FDM temperature at x = 4 mm is 27.86 °C at t = 10 s, while the cold-surface temperature remains approximately 25°C at the displayed precision. The point at x = 4 mm lies inside the insulation layer (whose geometric midpoint is at x = 5 mm). For perfect contact, a discontinuity in conductivity requires compatible one-sided temperature gradients at the interface. The plotted profile alone is insufficient to establish exact heat-flux continuity.

3.3.2. Temporal evolution characteristics of temperature

Fig. 3 shows temperature histories at four monitoring positions: the hot surface at x = 0 mm, the interface at x = 2 mm, an interior point of the insulation layer at x = = 4 mm, and the cold surface at x = 8 mm.

The hot-surface temperature is prescribed at 100°C after the boundary step. The reported FDM interface temperature at t = 10 s is 50.19°C, corresponding to a rise of 25.19°C. At x = 4 mm, the reported final temperature is 27.86°C, a rise of 2.86°C. The plotted cold-surface temperature remains close to its initial value over the 10 s interval. These results describe a short transient under the prescribed

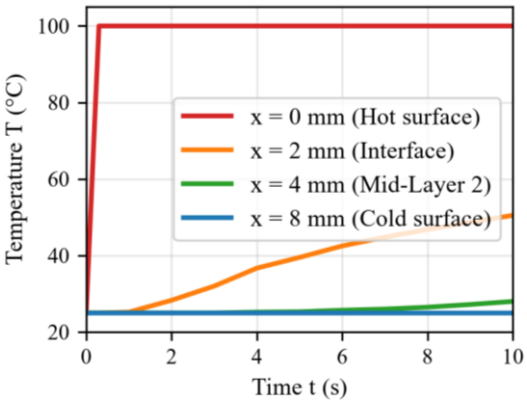

Fig. 3 Time-varying temperature curves of different positions

idealized conditions and do not establish long-duration insulation performance.

The apparent delay in the plotted temperature response reflects diffusion time scales, spatial and temporal discretization, and plotting resolution. The classical Fourier heat equation used here does not describe a sharp thermal front propagating at a finite speed. Consequently, an apparently unchanged curve should not be interpreted as proof of exactly zero temperature disturbance.

3.3.3. Evolution characteristics of heat flux density

Fig. 4 presents the heat-flux histories labeled at $x = 0.1$ mm, $x = 2$ mm, and $x = 7.9$ mm. The first and third locations are near the surfaces rather than on the boundaries. Heat flux is evaluated from Fourier's law using conductivity and a temperature gradient consistent with the local material and spatial discretization.

The plotted interface heat flux increases and then decreases slightly during the reported interval. The hot-side series is not separately distinguishable at the scale of the supplied plot, so no hot-surface peak is inferred here. The prescribed adiabatic condition constrains the flux at $x =$ = 8 mm; it does not by itself impose zero flux at the interior sampling location $x = 7.9$ mm.

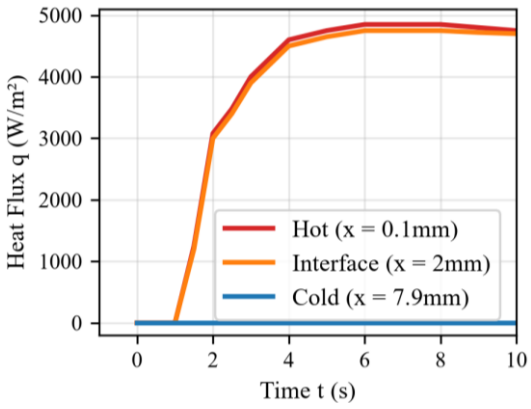

Fig. 4 Time-varying heat flux density curves of different positions

Notably, the transient heat flux varied at different structural positions during unsteady heat conduction. This phenomenon occurred because some of the thermal energy was stored within the structure as sensible heat. Uniform heat flux distribution along the thickness direction can only be achieved under steady-state heat conduction conditions.

4. Numerical Comparison with a Finite Element Model

4.1. Finite element model establishment

An Abaqus finite element model was used as a numerical reference for the same nominal bilayer geometry, material properties, initial temperature, and boundary conditions. The model used DC2D4 four-node planar heat-transfer elements with a stated global element size of 0.2 mm and a time increment of 0.05 s over 10 s. The FDM discretization reported in Section 3.2 uses 0.5 mm spacing and a nominal 0.278 s increment. Thus, the two discretizations are not identical, and their spatial and temporal discretization effects cannot be assumed to cancel. Numerical comparisons must use corresponding physical locations and times.

4.2. Comparative analysis of FDM and FEM calculation results

Fig. 5 presents the FEM spatial temperature profiles for comparison with Fig. 2. Both sets of profiles show heating from the prescribed hot boundary and decreasing temperature with depth. Quantitative agreement must be assessed using paired numerical outputs, since a visual similarity of trends does not establish equivalent temperature predictions.

For perfect thermal contact, the one-sided temperature gradients at the interface must satisfy heat-flux continuity. This is a local condition on conductivity-weighted gradients, not a conclusion that follows from similar overall curve shapes. Both methods should be evaluated for consistency with this condition.

The comparison addresses the stated transient conduction problem. It does not establish equivalence for all times, steady-state conditions, other layer combinations, or temperature-dependent material properties.

Fig. 6 presents the FEM histories at $x = 0$, 2, 4, and 8 mm for comparison with Fig. 3. The point at $x = 4$ mm is an interior monitoring location in layer 2, not its geometric midpoint.

Agreement at the prescribed hot-surface temperature is expected because the same Dirichlet condition is imposed in both models. The interior temperature histories

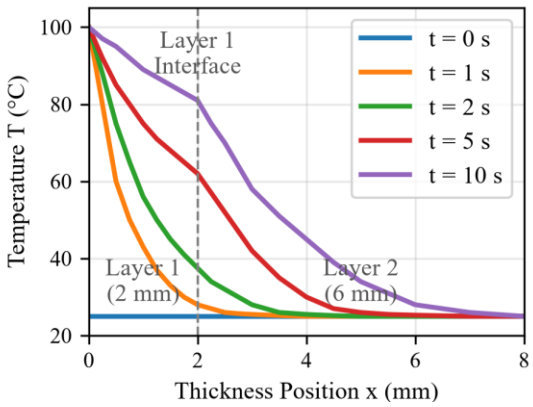

Fig. 5 Temperature distribution along the thickness at different moments (FEM)

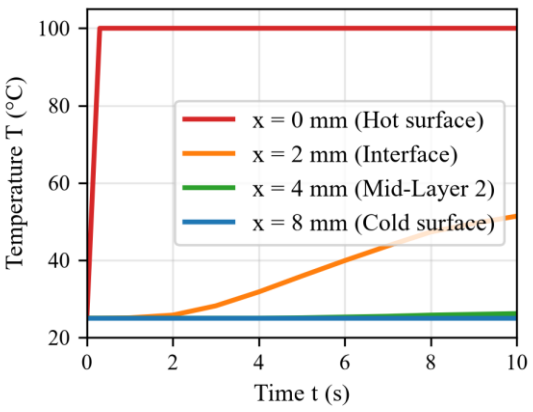

Fig. 6 Time-varying temperature curves of different positions (FEM)

provide a more informative comparison of transient behavior. Quantitative assessment requires consistent sampling times and extraction locations; agreement at the boundary alone does not demonstrate the accuracy of the interior solution or the absence of accumulated numerical error.

4.3. Quantitative comparison at the final transient time of 10 s

4.3.1. Error evaluation indicators

Differences between the FDM and FEM predictions are described using absolute temperature difference and a temperature-rise-normalized relative difference. The FEM result is treated as a numerical reference, not as an exact or measured temperature. The absolute difference is defined by Eq. (8)

$$\Delta T = \left| T_{FDM} - T_{FEM} \right|. \tag{8}$$

For monitoring points with a nonzero FEM temperature rise, the relative difference is normalized by that rise as in Eq. (9)

$$\delta = \frac{\left| T_{FDM} - T_{FEM} \right|}{\left| T_{FEM} - T_0 \right|} \times 100\%. \tag{9}$$

Here, the FDM and FEM temperatures are evaluated at the same location and time, and $T_0 = 25$°C. The denominator uses the FEM temperature rise consistently. The relative difference is reported as N/A when the reference rise is zero; near-zero rises make this ratio sensitive to rounding. Absolute differences should therefore be reported alongside normalized values. Neither metric measures error relative to an experiment.

4.3.2. Differences calculated from the tabulated final temperatures

Table 2 retains the reported final temperatures and lists the differences calculated from those displayed values. These pointwise statistics are restricted to $t = 10$ *s* and do not represent maxima over the full space-time solution. Rounding of the temperatures to two decimal places also limits the precision of the derived statistics.

4.3.3. Interpretation and limits of the comparison

Using the displayed temperatures in Table 2, the largest absolute difference among the listed locations is 0.11°C at the interface. The largest defined relative difference is approximately 1.42% at $x = 4$ mm, because normalization uses the smaller local FEM temperature rise. These are different statistics and occur at different locations. No universal 5% acceptance threshold is assumed. Pointwise agreement cannot establish grid independence, exclude systematic bias, or prove that the numerical implementation is free of errors.

4.4. Scope of numerical verification

The purpose of the FDM–FEM comparison is to assess numerical consistency for the stated bilayer problem. A reliable assessment requires agreement between the tabulated values, spatial profiles, and time histories, together with evidence that the conclusions are insensitive to further mesh and time-step refinement.

Table 2

Pointwise FDM–FEM differences based on the reported temperatures at $t = 10$ s

Monitoring position	FDM Temperature, °C	FEM Temperature, °C	Absolute error ΔT, °C	Relative error δ, %
Hot surface $x = 0$ mm	100.00	100.00	0.00	0.00
Layer interface $x = 2$ mm	50.19	50.08	0.11	0.44
Insulation layer middle $x = 4$ mm	27.86	27.82	0.04	1.42
Cold surface $x = 8$ mm	25.00	25.00	0.00	N/A

The reported final-time pointwise differences provide a limited comparison between numerical outputs. They do not establish a global error bound, prove equivalence between the two methods, or independently demonstrate the physical accuracy of the model.

The intended contribution of the dedicated FDM program is a convenient parameter-driven workflow for one-dimensional multilayer conduction problems. Its practical value lies in simplifying repeated model setup and result visualization. Any claim of a computational speed advantage requires timings obtained with a defined workload, hardware configuration, and accuracy target.

Numerical verification and experimental validation have different objectives. The present comparison concerns numerical solutions of the same idealized conduction problem. Validation against measured temperatures has not been performed and remains planned future work; therefore, predictive accuracy for physical specimens is not established here.

4.5. Potential sources of numerical difference

The differences discussed here concern numerical solutions rather than deviations from measurements. Their causes cannot be uniquely identified from a small set of final-time temperatures.

Potential contributions include spatial and temporal discretization, interface treatment, boundary implementation, and output interpolation. Their relative importance requires controlled sensitivity studies.

1. Spatial and temporal discretization. Within a smooth homogeneous region, FTCS is first order in time and second order in space. Abaqus/Standard transient pure-conduction analysis uses backward Euler time integration. Differences between the results cannot be assigned solely to the FDM temporal order, especially when the meshes and time increments differ.

2. Stability and refinement. Satisfying the FTCS stability criterion does not establish discretization accuracy or exclude cumulative error. Spatial and temporal refinement studies are needed to assess the sensitivity of the

reported temperatures.

3. Interface and boundary treatment. Conductivity is discontinuous at the layer interface, so the discretization must represent the associated flux condition explicitly. The adiabatic boundary approximation and the extraction of near-boundary heat fluxes also require consistency checks.

The present comparison does not isolate these contributions or rule out shared modeling assumptions and implementation errors. A discrete energy-balance check and comparisons using successively refined discretizations would strengthen numerical verification without requiring new physical experiments.

4.6. Practical scope and limitations

Abaqus offers a general-purpose framework for heat-transfer analysis, including geometries and physical effects beyond the present one-dimensional case. Its standard implicit transient integration is unconditionally stable for linear problems, but stability does not remove the need to assess temporal and spatial accuracy.

The dedicated FDM program provides a focused interface for specifying layers, applying prescribed thermal loads, and visualizing transient temperatures. Its explicit scheme is simple, but the allowable time increment decreases with the square of grid spacing. No numerical speedup factor is claimed because a controlled runtime comparison is not reported.

5. Conclusions

A parametric program based on explicit finite differences was developed for transient one-dimensional heat conduction in multilayer plates. The bilayer case illustrates the calculation of spatial temperature profiles and temperature histories at selected locations. Comparison with an Abaqus model provides a framework for assessing numerical consistency under prescribed conditions. The reported pointwise statistics do not establish equivalence over the complete temperature field and time history, and the present study does not claim a verified global error bound or a measured computational speed advantage.

The present work is a preliminary numerical study with constant layer properties and idealized thermal boundary and contact conditions. Experimental validation has not been performed because suitable testing conditions are currently unavailable. Future work will compare predictions with transient temperature measurements when testing becomes feasible. Mesh and time-step convergence, interface flux conservation, and energy balance remain important numerical verification requirements for extending the method to additional cases.

Funding

This study was financially supported by the Qingdao Huanghai University High-level Scientific Research Cultivation Project 2025GJPY01 and the Natural Science Foundation of Shandong Province (ZR2023QE292). The support is gratefully acknowledged.

References

1. **Anderson Jr, J. D.** 2006. Hypersonic and high-temperature gas dynamics. 2nd ed. Reston, VA: American Institute of Aeronautics and Astronautics. 813p. http://dx.doi.org/10.2514/4.861956.
2. **Bertin, J. J.; Cummings, R. M.** 2006. Critical hypersonic aerothermodynamic phenomena, Annual Review of Fluid Mechanics 38: 129-157. https://doi.org/10.1146/annurev.fluid.38.050304.092041.
3. **Knight, D.; Chazot, O.; Austin, J.; Badr, M. A.; Candler, G.; Celik, B.; de Rosa, D.; Donelli, R.; Komives, J.; Lani, A.; Levin, D.; Nompelis, I.; Panesi, M.; Pezzella, G.; Reimann, B.; Tumuklu, O.; Yuceil, K.** 2017. Assessment of predictive capabilities for aerodynamic heating in hypersonic flow, Progress in Aerospace Sciences 90: 39-53. https://doi.org/10.1016/j.paerosci.2017.02.001.
4. **Bianco, V.; Chiacchio, F.; Manca, O.; Nardini, S.** 2009. Numerical investigation of nanofluids forced convection in circular tubes, Applied Thermal Engineering 29(17-18): 3632-3642. https://doi.org/10.1016/j.applthermaleng.2009.06.019.
5. **Zhu, M.; Wang, S.G.; Huang, H.; Huang, G.; Wu, F.; Sun, S.H.; Li, B.; Xu, Z.J.** 2021. Numerical and experimental study on the response characteristics of warhead in the fast cook-off process, Defence Technology 17(4): 1444-1452. https://doi.org/10.1016/j.dt.2020.08.001.
6. **Uyanna, O.; Najafi, H.** 2020. Thermal protection systems for space vehicles: A review on technology development, current challenges and future prospects, Acta Astronautica 176: 341-356. https://doi.org/10.1016/j.actaastro.2020.06.047.
7. **Lu, T. J.; Valdevit, L.; Evans, A. G.** 2005. Active cooling by metallic sandwich structures with periodic cores, Progress in Materials Science 50(7): 789-815. https://doi.org/10.1016/j.pmatsci.2005.03.001.
8. **Pierre, A. C.; Pajonk, G. M.** 2002. Chemistry of aerogels and their applications. Chemical Reviews, 102(11): 4243-4266. http://dx.doi.org/10.1021/cr0101306.
9. **Hrubesh, L. W.; Pekala, R. W.** 1994. Thermal properties of organic and inorganic aerogels, Journal of Materials Research 9(3): 731-738. https://doi.org/10.1557/JMR.1994.0731.
10. **Krenkel, W. (Ed.)** 2008. Ceramic matrix composites: Fiber reinforced ceramics and their applications. Weinheim: Wiley-VCH. 440p. http://dx.doi.org/10.1002/9783527622412.
11. **Blosser, M. L.** 2013. Mass Efficiency Considerations for Thermally Insulated Structural Skin of an Aerospace Vehicle, Journal of Thermophysics and Heat Transfer 27(3): 429-434. http://dx.doi.org/10.2514/1.T4008.
12. **Glass, D. E.** 2008. Ceramic Matrix Composite (CMC) Thermal Protection Systems (TPS) and Hot Structures for Hypersonic Vehicles, 15th AIAA International Space Planes and Hypersonic Systems and Technologies Conference, art. no. AIAA 2008-2682. http://dx.doi.org/10.2514/6.2008-2682.
13. **Dong, W.; Deng, P.; Lin, S.; Chen, T.** 2023. Numerical study of a new scheme of self-adaptive transpiration cooling, Applied Thermal Engineering 230: 120779. https://doi.org/10.1016/j.applthermaleng.2023.120779.
14. **Spinnler, M.; Winter, E. R. F.; Viskanta, R.;**

Sattelmayer, T. 2004. Theoretical studies of high-temperature multilayer thermal insulations using radiation scaling, Journal of Quantitative Spectroscopy and Radiative Transfer 84(4): 477-491. https://doi.org/10.1016/S0022-4073(03)00264-4.
15. **Klett, J. W.; Ervin, V. J.; Edie, D. D.** 1999. Finite-element modeling of heat transfer in carbon/carbon composites, Composites Science and Technology 59(4): 593-607. https://doi.org/10.1016/S0266-3538(98)00099-2.
16. **Souayfane, F.; Fardoun, F.; Biwole, P. H.** 2016. Phase change materials (PCM) for cooling applications in buildings: A review, Energy and Buildings 129: 396-431. https://doi.org/10.1016/j.enbuild.2016.04.006.
17. **Yagi, S.; Kunii, D.; Wakao, N.** 1960. Studies on axial effective thermal conductivities in packed beds, AIChE Journal 6(4): 543-546. https://doi.org/10.1002/aic.690060407.
18. **Liu, X.; Peng, B.; Yu, W.** 2021. Multiscale modeling of the effective thermal conductivity of 2D woven composites by mechanics of structure genome and neural networks, International Journal of Heat and Mass Transfer 179: 121673. https://doi.org/10.1016/j.ijheatmasstransfer.2021.121673.
19. **Yang, J.; Liu, M.** 2017. A wall grid scale criterion for hypersonic aerodynamic heating calculation, Acta Astronautica 136: 137-143. https://doi.org/10.1016/j.actaastro.2016.11.043.
20. **Kumar, S.; Mahulikar, S. P.** 2016. Selection of materials and design of multilayer lightweight passive thermal protection system, ASME Journal of Thermal Science and Engineering Applications 8(2): 021003. https://doi.org/10.1115/1.4031737.
21. **Liu, Y.; Zhao, H.; Liu, K.; Zhao, Z.; Feng, M.; Chen, J.** 2026. Multi-scale modeling: Analysis and design of thermal-mechanical coupling behavior of integrated thermal protection systems, Chinese Journal of Aeronautics 39(3): 103855. https://doi.org/10.1016/j.cja.2025.103855.
22. **Audet, C.; Dennis, J. E., Jr.** 2006. Mesh Adaptive Direct Search Algorithms for Constrained Optimization, SIAM Journal on Optimization, 17(1): 188-217. https://doi.org/10.1137/040603371.
23. **Lobbia, M. A.** 2017. Multidisciplinary Design Optimization of Waverider-Derived Crew Reentry Vehicles, Journal of Spacecraft and Rockets, 54(1): 233-245. http://dx.doi.org/10.2514/1.A33253.
24. **Wang, F.; Hu, Y.; Zhang, B.; Zha, Y.; Luo, X.** 2025. Fast Temperature Field Extrapolation Under Non-Periodic Boundary Conditions, Applied Sciences 15(7): 3895. https://doi.org/10.3390/app15073895.

J. Wang, J. Ma, G. Xue, P. Yang, P. Zhao, R. Yu, R. Yang

NUMERICAL SIMULATION OF HEAT CONDUCTION IN MULTI-LAYER PLATE THERMAL INSULATION STRUCTURES BASED ON EXPLICIT FINITE DIFFERENCE METHOD

S u m m a r y

This study presents a parametric program for transient one-dimensional heat conduction in multilayer plates using the explicit Forward-Time Central-Space finite-difference scheme. The program accepts layer thicknesses, thermophysical properties, and prescribed temperature boundary conditions, and provides spatial temperature profiles and histories at selected monitoring locations. A PySide6 graphical interface supports parameter entry and result visualization. A bilayer structure with a 2 mm ceramic layer and a 6 mm aerogel composite layer is considered over a 10 s heating interval. An Abaqus finite element model is used for a numerical comparison under the same nominal physical conditions. The comparison is intended to evaluate inter-solver consistency; pointwise temperature differences do not establish a global error bound or experimental predictive accuracy. The scope is preliminary numerical analysis, and validation against measured temperatures is planned for future work. The program provides a basis for parameter-driven investigation of idealized multilayer conduction problems.

Keywords: multi-layer thermal insulation plate, transient heat conduction, explicit finite difference method, parametric simulation, program development.

Received August 18, 2026
Accepted October 15, 2026



This article is an Open Access article distributed under the terms and conditions of the Creative Commons Attribution 4.0 (CC BY 4.0) License (http://creativecommons.org/licenses/by/4.0/).